

11. Denk, W., Webb, W. W. & Hudspeth, A. J. Mechanical properties of sensory hair bundles are reflected in their Brownian motion measured with a laser differential interferometer. *Proc. Natl Acad. Sci. USA* **86**, 5371–5375 (1989).
12. Svoboda, K., Schmidt, C. F., Schnapp, B. J. & Block, S. M. Direct observation of kinesin stepping by optical trapping interferometry. *Nature* **365**, 721–727 (1993).
13. Kojima, H., Muto, E., Higuchi, H. & Yanagida, T. Mechanics of single kinesin molecules measured by optical trapping nanometry. *Biophys. J.* **73**, 2012–2022 (1997).
14. Allersma, M. W., Gittes, F., deCastro, M. J., Stewart, R. J. & Schmidt, C. F. Two-dimensional tracking of ncd motility by back focal plane interferometry. *Biophys. J.* **74**, 1074–1085 (1998).
15. Pralle, A., Prummer, M., Florin, E. L., Stelzer, E. H. & Horber, J. K. Three-dimensional high-resolution particle tracking for optical tweezers by forward scattered light. *Microsc. Res. Tech.* **44**, 378–386 (1999).
16. Mason, T. G., Ganesan, K., Van Zanten, J. H., Wirtz, D. & Kuo, S. C. Particle tracking microrheology of complex fluids. *Phys. Rev. Lett.* **79**, 3282–3285 (1997).
17. Yamada, S., Wirtz, D. & Kuo, S. C. Mechanics of living cells measured by laser tracking microrheology. *Biophys. J.* **78**, 1736–1747 (2000).
18. McGrath, J. L., Hartwig, J. H. & Kuo, S. C. The mechanics of F-actin microenvironments depend on the chemistry of probing surfaces. *Biophys. J.* (in the press) (2000).
19. Gerbal, F. et al. On the 'Listeria' propulsion mechanism. *Pramana. J. Phys.* **53**, 155–170 (1999).
20. Kuo, S. C., Gelles, J., Steuer, E. & Sheetz, M. P. A model for kinesin movement from nanometer-level movements of kinesin and cytoplasmic dynein and force measurements. *J. Cell Sci.* **14** (suppl.), 135–138 (1991).
21. Olbris, D. J. & Herzfeld, J. Reconstitution of *Listeria* motility: implications for the mechanism of force transduction. *Biochim. Biophys. Acta* **1495**, 140–149 (2000).
22. Gerbal, F. et al. Measurement of the elasticity of the actin tail of *Listeria monocytogenes*. *Eur. Biophys. J.* **29**, 134–140 (2000).
23. Reif, F. *Fundamentals of Statistical and Thermal Physics* (McGraw-Hill, New York, 1965).
24. Qian, H., Sheetz, M. P. & Elson, E. L. Single particle tracking: Analysis of diffusion and flow in two-dimensional systems. *Biophys. J.* **60**, 910–921 (1991).
25. Molloy, J. E., Burns, J. E., Kendrick-Jones, J., Tregear, R. T. & White, D. C. Movement and force produced by a single myosin head. *Nature* **378**, 209–212 (1995).
26. Mehta, A. D., Finer, J. T. & Spudich, J. A. Detection of single molecule interactions using correlated thermal diffusion. *Proc. Natl Acad. Sci. USA* **94**, 7927–7931 (1997).
27. Dupuis, D. E., Guilford, W. H., Wu, J. & Warshaw, D. M. Actin filament mechanics in the laser trap. *J. Muscle Res. Cell Motil.* **18**, 17–30 (1997).
28. Portnoy, D. A., Jacks, P. S. & Hinrichs, D. J. Role of hemolysin for the intracellular growth of *Listeria monocytogenes*. *J. Exp. Med.* **167**, 1459–1471 (1988).

Supplementary information is available on Nature's World-Wide Web site (<http://www.nature.com>) or as paper copy from the London editorial office of Nature.

Acknowledgements

We thank L. Machesky for J774 cells, and D. Portnoy and J. Skoble for *Listeria* strains and general advice. We also thank the National Science Foundation, the National Institutes of Health and the Whitaker Foundation for their support. J.L.M. was supported as a BME Distinguished Postdoctoral Fellow, partially funded by the Whitaker Foundation.

Correspondence and requests for materials should be addressed to S.C.K. (e-mail: skuo@bme.jhu.edu).

Crystal structure of fibroblast growth factor receptor ectodomain bound to ligand and heparin

Luca Pellegrini*, David F. Burke*, Frank von Delft*, Barbara Mulloy† & Tom L. Blundell*

* Department of Biochemistry, University of Cambridge, 80 Tennis Court Road, Cambridge, CB2 1GA, UK

† National Institute for Biological Standards and Control, South Mimms, Potters Bar, EN6 3QG, UK

Fibroblast growth factors (FGFs) are a large family of structurally related proteins with a wide range of physiological and pathological activities¹. Signal transduction requires association of FGF with its receptor tyrosine kinase (FGFR)² and heparan sulphate proteoglycan in a specific complex on the cell surface. Direct involvement of the heparan sulphate glycosaminoglycan polysaccharide in the molecular association between FGF and its receptor is essential for biological activity^{3–5}. Although crystal structures of

binary complexes of FGF–heparin^{6,7} and FGF–FGFR^{8,9} have been described, the molecular architecture of the FGF signalling complex has not been elucidated. Here we report the crystal structure of the FGFR2 ectodomain in a dimeric form that is induced by simultaneous binding to FGF1 and a heparin decasaccharide. The complex is assembled around a central heparin molecule linking two FGF1 ligands into a dimer that bridges between two receptor chains. The asymmetric heparin binding involves contacts with both FGF1 molecules but only one receptor chain. The structure of the FGF1–FGFR2–heparin ternary complex provides a structural basis for the essential role of heparan sulphate in FGF signalling.

We reconstituted the ligand-binding extracellular region of human FGFR2 (splice variant IIIc) as a ternary complex with human FGF1 and a heparin decasaccharide by mixing the three components in a 2:2:1 stoichiometric ratio. The ternary complex eluted as a single peak at the expected relative molecular mass of 83,600 (*M*_r 83.6K) on size-exclusion chromatography. The complex was crystallized and its structure determined by X-ray crystallography at 2.8 Å using multiple anomalous dispersion based on selenomethionine substitution of the receptor moiety (Table 1).

Analysis of the crystals shows that one heparin decasaccharide links two FGF1 molecules, each of which binds a receptor ectodomain, unambiguously defining a heteropentameric assembly, consistent with the *in vitro* reconstitution (Fig. 1a, b). The complex can alternatively be considered as two 1:1 FGF1–FGFR2 complexes associated through interaction with the heparin. The ligand-binding fragment of FGFR2 comprises two immunoglobulin-like domains, D2 (residues 152–249) and D3 (residues 254–360), separated by a short linker (residues 250–253)^{8,9} (Fig. 1c). D2 belongs to the I class, whereas D3 approximates to a class C2 fold. FGF1 adopts the well-characterized β-trefoil fold¹⁰. The two receptor chains in the ternary complex show marked bends in the linker regions, with angles of 106° and 87° between D2 and D3. The two protein halves of the complex are related by an approximate two-fold symmetry axis, which we expect would lie perpendicular to the membrane in the cell. The root-mean square deviation (r.m.s.d.) for the Cα superposition of the two halves of the complex is 2.8 Å, whereas the r.m.s.d. for the 230 Cα atoms of FGF1 and D2 is 1.0 Å.

There are two 1:1 FGF–FGFR binary complexes within the heteropentamer, which we refer to as A and B. In A both ligand and receptor interact with heparin, whereas in B only the ligand is in contact with heparin. The entire length of the protein-bound heparin decasaccharide is visible in the experimental electron-density map (Fig. 2a). Heparin lies between and interacts with the two FGF1 molecules, but is tilted away from the quasi-dyad so that it extends past the ligand dimer to interact only with receptor ectodomain A (Figs 1a, b and 3a). The heparin helix presents a marked distortion that has not been observed in previous structural studies of FGF–heparin complexes^{6,7}. The helical axis shows a 34° kink between disaccharides 2 and 3, accompanied by a decreased helical rise between disaccharide 2 and 3 (7.1 Å) and between 3 and 4 (7.9 Å) (for numbering of heparin disaccharide units see Fig. 2b). The total surface area buried at the protein–heparin interface is large at 2,240 Å² (617 Å² with FGF1 and 631 Å² with domain D2 in A; 992 Å² with FGF1 in B). van der Waals contacts contribute substantially to the protein–heparin interactions as suggested previously¹¹. FGF1 binding to heparin is mediated by a set of basic and polar residues, Asn 18, Lys 112, Lys 113, Asn 114, Lys 118, Arg 119, Arg 122, Gln 127 and Lys 128, which were identified in previous structural and mutagenesis experiments^{6,7,11}. FGF1 in binary complex A interacts with six monosaccharides, from iduronic acid in disaccharide 1 (IdoA-1) to glucosamine in disaccharide 4 (GlcN-4), whereas FGF1 in B interacts with five monosaccharides, from GlcN-1 to GlcN-3 (Fig. 2b).

In the structure of the ternary complex, heparin links two FGF1 molecules into a dimer that lacks a protein–protein interface, in a

similar fashion to that previously reported⁷, but with significant differences in the relative orientation of FGF and heparin. Superposition of PDB entry 2AXM (ref. 7) with the heparin-linked FGF1 dimer of the heteropentamer shows that a good agreement is obtained for FGF1 in A and the heparin. However, FGF1 in B is rotated by about 120° relative to the second FGF1 protomer of 2AXM around an axis roughly aligned with the pseudo three-fold axis of the β-trefoil (Fig. 3b). FGF1 in B is thus able to make an

additional set of contacts with heparin, while remaining in contact with it through the heparin-binding loop. Conserved Trp 107 is central to this new heparin-binding site (Fig. 2c). An FGF2 mutant, in which the tryptophan residue was mutated to alanine, showed unaltered affinity for the receptor, but a marked reduction in mitogenic potency¹². It was originally proposed that the amino-acid sequence of the loop containing the tryptophan residue constituted a secondary receptor-binding site¹². Our structure

Table 1 Crystallographic analysis

Diffraction data (space group, $P6_2$; $a = b = 195.90 \text{ \AA}$, $c = 68.86 \text{ \AA}$)									
Data set	Resolution (Å)	Wavelength (Å)	Reflections (unique)	Redundancy	Completeness (outer shell)	R_{sym} (%)† (outer shell)	$I/\sigma(I)$ (outer shell)	Beamline	
Se–Met (remote)	3.5	0.93928	281,374 (37,018*)	7.6	99.8 (100.0)	11.2 (36.8)	17.1 (3.5)	19-ID	
Se–Met (peak)	3.5	0.97924	281,407 (37,767*)	7.7	99.9 (100.0)	11.8 (43.0)	14.8 (2.6)	19-ID	
Se–Met (edge)	3.5	0.97940	282,931 (36,963*)	7.5	99.9 (100.0)	10.8 (26.1)	13.3 (5.6)	19-ID	
Native	2.8	1.00	127,885 (36,432)	3.5	98.3 (100.0)	8.4 (47.4)	13.7 (1.7)	5.2R	
MAD phasing									
	Se–Met (remote)	Se–Met (peak)	Se–Met (edge)						
Rcullis‡ (iso/ano)	–/0.90	0.61/0.74	0.70/0.77						
Phasing power§ (iso/ano)	–/0.78	1.79/1.86	1.45/1.85						
Refinement¶									
Resolution (Å)	Reflections	Number of non-H atoms	R factor (%)¶	Free R factor (%)	Average B (Å ²)	R.m.s.d. bonds (Å)	R.m.s.d. angles (degrees)	R.m.s.d. bonded B (Å ²)	
24.2–2.8	36,348	5,247	24.2	28.0	69.1	0.009	1.52	5.36	

* For MAD data, the Bijvoet pairs were not merged.

† $R_{\text{sym}} = \sum_{hkl} \sum_j |I_j(hkl) - \langle I(hkl) \rangle| / \sum_{hkl} \sum_j I_j(hkl)$

‡ Rcullis as defined in SHARP.

§ Phasing power as defined in SHARP.

¶ Statistics for data with $F > 3\sigma$.

¶ R factor = $\sum_{hkl} ||F_{\text{obs}}| - |F_{\text{calc}}|| / \sum_{hkl} |F_{\text{obs}}|$

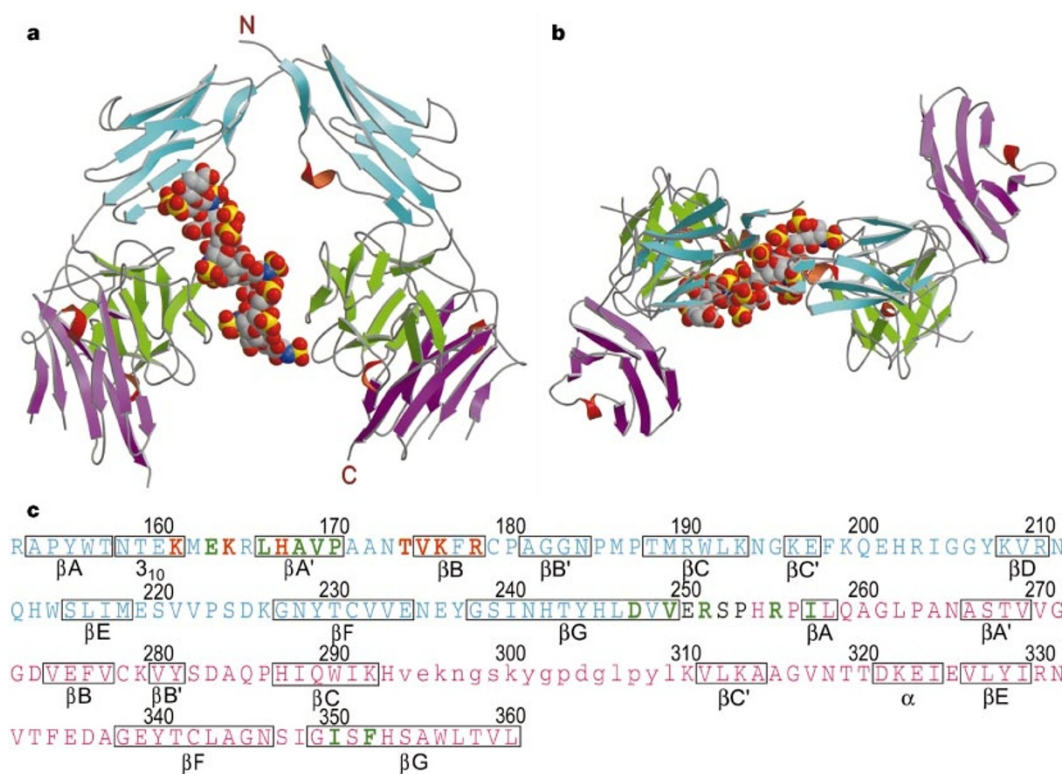


Figure 1 The FGF1–FGFR2–heparin complex. **a**, View perpendicular to the approximate dyad of the complex. FGFR2 domains 2 (D2) and 3 (D3) are cyan and magenta, respectively, and FGF1 is green. The heparin molecule is in CPK representation. **b**, View along the dyad. **c**, Amino-acid sequence of the ligand-binding region of human FGFR2.

Domains D2 and D3 are coloured as in **a**. Residues that interact with heparin and FGF1 are highlighted in red and green, respectively. Regions of secondary structure are boxed. β-strands, α-helices and 3_{10} helices are indicated below the relative sequence. D3 residues 294–309, which were disordered in the crystals, are in lower case.

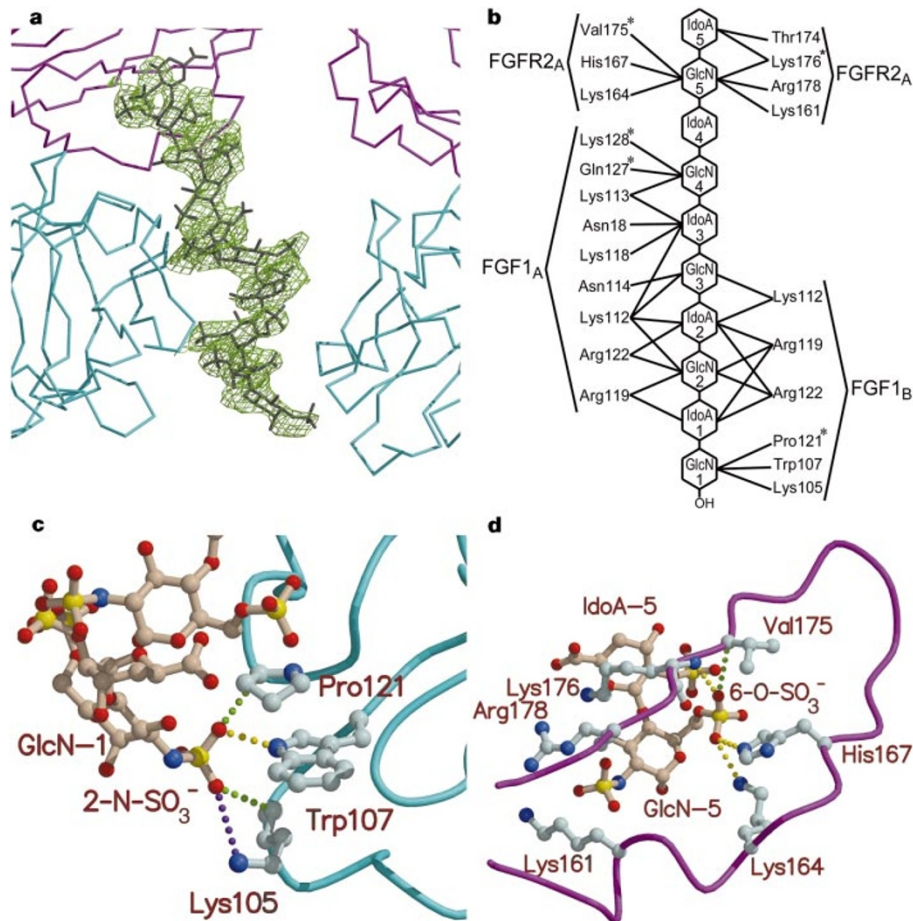


Figure 2 Heparin-protein interactions in the FGF1-FGFR2-heparin complex. **a**, Experimental 3.0 Å electron density of the heparin deca-saccharide contoured at 1.2σ. **b**, Summary of heparin-protein interactions. The five disaccharides of the heparin deca-saccharide are numbered from the reducing end, indicated by a hydroxyl group. Each disaccharide begins with glucosamine (GlcN) followed by iduronic acid (IdoA). Solid lines represent interactions between amino acids and monosaccharide(s). Heparin comes in

close contact with the backbone atoms of amino acids marked by an asterisk. **c**, Details of the FGF1-heparin interaction in binary complex B. Heparin and amino-acid side chains are shown as a ball-and-stick model and the protein backbone as a coil. Dashed lines represent hydrogen bonds (yellow), van der Waals contacts (green) and electrostatic interactions (purple). **d**, FGFR2-heparin interactions. Only heparin disaccharide 5 is depicted for clarity. Dashed lines coloured as in **c**.

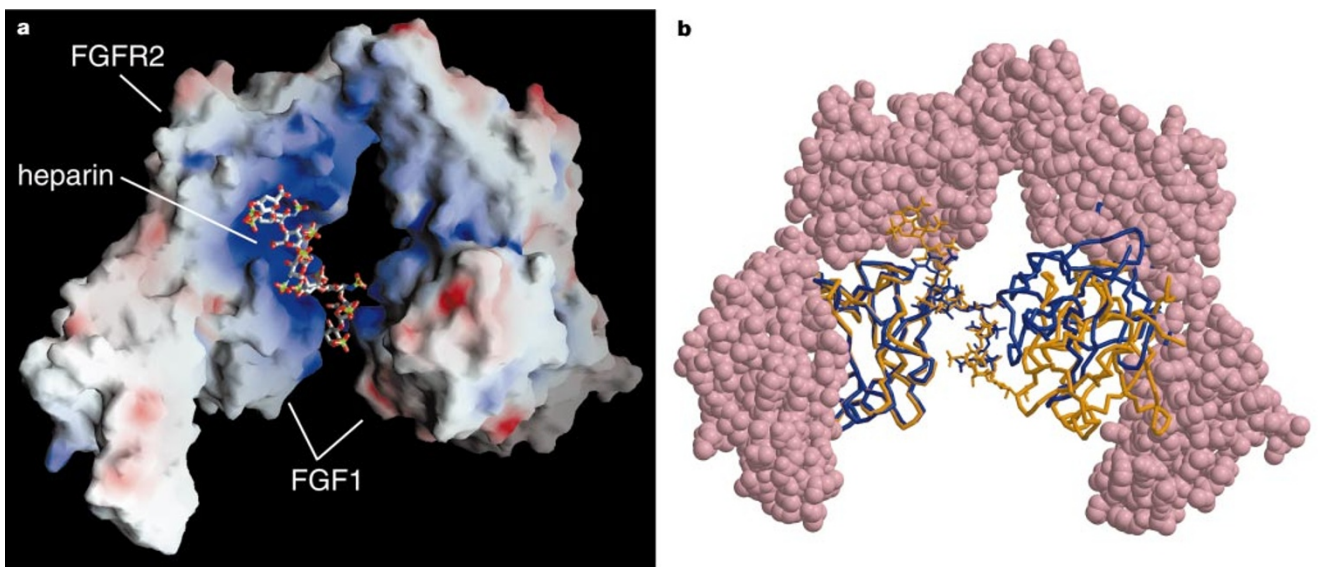


Figure 3 Overall architecture of the FGF1-FGFR2-heparin complex. **a**, Electrostatic potential of the heparin-binding site in the FGF1-FGFR2-heparin complex, mapped onto a molecular surface rendition of the complex. The heparin is shown as a stick model. In the ternary complex, the heparin deca-saccharide is surrounded by regions of positive

charge (blue represents +20e per Å²). **b**, Superposition of heparin-linked FGF1 dimers. The dimer from the FGF1-FGFR2-heparin complex is yellow, the PDB entry 2AXM is blue. The FGFR2 ectodomains are shown in CPK representation.

shows that the N-sulphate group of GlcN-1 is hydrogen bonded to Trp 107 and comes in close contact with Pro 121 and Lys 105, which are stacked above and below the tryptophan side chain (Fig. 2c). This interaction might be important for the correct positioning of

FGF1 relative to heparin and thus for the recruitment of a second binary complex into an active heteropentamer.

The heparin-binding region of FGFR2 observed in the structure of the ternary complex comprises residues in the highly conserved

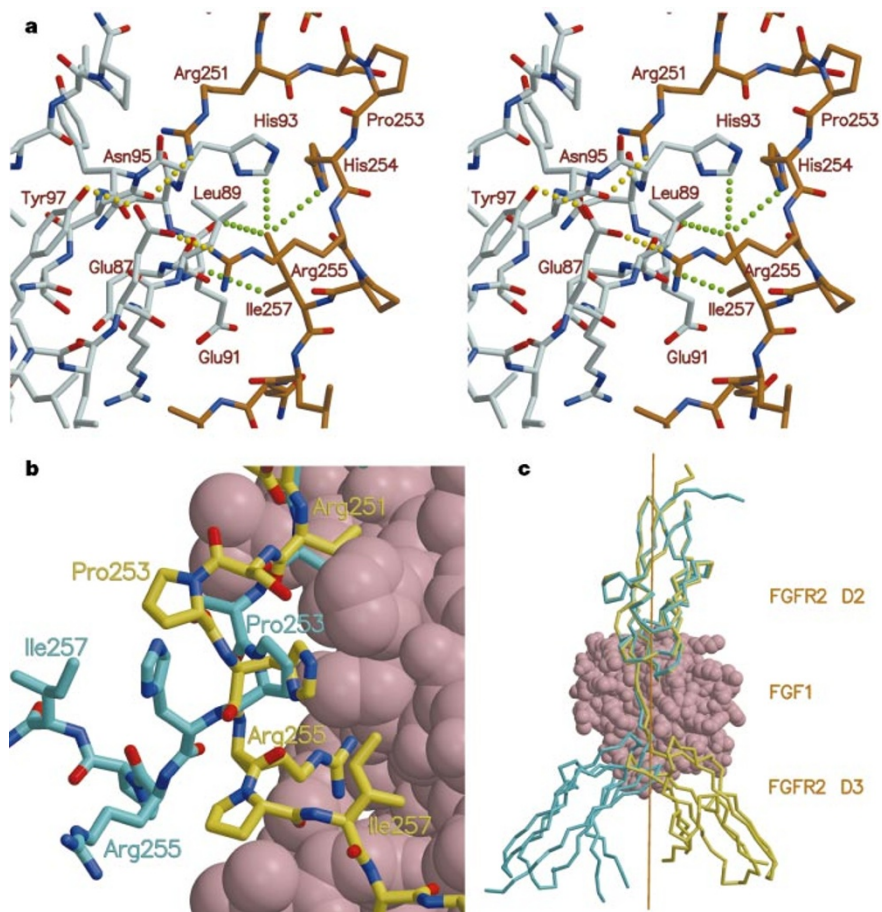


Figure 4 Ligand–receptor interactions in FGF–FGFR complexes with and without heparin. **a**, Stereoview of the ligand–receptor interface in the FGF1–FGFR2–heparin complex. The receptor is brown and the ligand is light grey. Dashed lines represent hydrogen bonds (yellow) and van der Waals contacts (green). **b**, Close-up of FGFR2 sequence R251–S–P–H–R–P–I257, illustrating the different conformation of the polypeptide chain in FGF–FGFR complexes with (binary complex A; yellow) and without

(PDB entry 1DJS; cyan) heparin. FGF1 is in CPK representation. **c**, Superposition of FGFR2 ectodomains showing the different orientation of D3 in FGF–FGFR complexes with and without heparin. The C α trace of FGFR2 ectodomain from binary complex A (yellow) is superimposed on that of PDB entry 1DJS (cyan). FGF1 is also shown in CPK representation. The rotation axis that relates the two D3 domains is drawn.

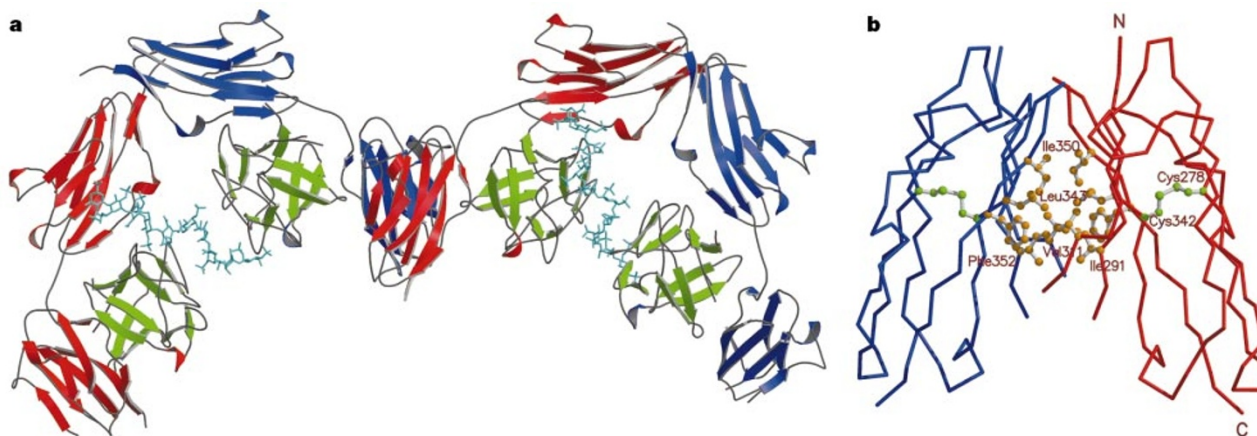


Figure 5 Higher order FGFR oligomerization as observed in crystals of the FGF1–FGFR2–heparin complex. **a**, Crystal packing of neighbouring heteropentamers. Linking successive heteropentamers together by apposition of D3 domains generates the hexagonal symmetry in the crystals. FGFR2 ectodomains are red and blue, FGF1 is green

and heparin is cyan. **b**, Face-to-face interaction between FGFR D3 domains belonging to neighbouring heteropentamers. The protein backbone is depicted as a C α trace, the hydrophobic residues at the D3–D3 interface and the disulphide bridge of each D3 domain are shown as ball-and-stick models.

sequence K161-M-E-K-R-L-H-A-V-P-A-A-N-T-V-K-F-R178, which has been identified as being essential for heparin binding¹³ (Figs 1c and 2b, d). All basic residues in this sequence, with the exception of Arg 165, are involved in interactions with the sulphate groups of GlcN-5 or the carboxylate group of IdoA-5. Both sugars in disaccharide 5 come into close contact with the receptor surface. The 6-O-sulphate group of GlcN-5 is involved in a particularly large range of interactions, including hydrogen bonds to Lys 164, His 167 and the backbone amide of Lys 176, and a van der Waals contact with Thr 174 and Val 175 (Fig. 2d). This is in agreement with reports that 6-O-desulphated heparin retains its ability to bind FGF, but blocks receptor binding and mitogenic activity¹⁴. The role of Lys 164 in neutralizing the 6-O-sulphate group of GlcN-5 appears particularly important as the sulphate group is partially buried.

The structure of the ternary complex shows that a heparin span of eight hexoses would still be capable of crosslinking ligand and receptor, through interactions of Lys 161 with the 2-O-sulphate group of IdoA-4 and Lys 164 with the carboxylate function of IdoA-4, albeit presumably with reduced efficacy. Our structure predicts that maximization of the heparin–protein interactions in the ternary complex would be achieved with a heparin fragment spanning twelve sugars: a dodecasaccharide should be able to make an additional set of contacts with Lys 208 and Arg 210 on β -strand D of domain D2 (Fig. 1c). These observations are in agreement with biochemical data that indicate that an octasaccharide is the minimal heparin length required to support FGF physiological activity¹⁵ and that a dodecasaccharide is equivalent to whole heparin in FGF1 proliferation potency¹⁶.

Protein–protein interactions in the ternary complex are dominated by ligand binding of each receptor chain. FGF1 binding to the receptor involves contacts with D2, the linker region and residues 254–260 of D3, which create a continuous interface burying a total of 1,700 Å² surface area. This is consistent with biochemical evidence that narrows the minimal ligand-binding region of FGFR to a fragment comprising D2, the interdomain sequence and an amino-terminal sequence of D3 (ref. 17). Contacts between FGF1 and domain D2 are predominantly hydrophobic and involve residues Tyr 15, Gly 20, Phe 22, Tyr 94, Leu 133 and Leu 135 of the ligand, and residues Lys 164, Leu 166, Ala 168, Val 169 and Pro 170 of D2. Interactions of an electrostatic nature are those of Glu 163 and Asp 247 of FGFR2 with Arg 35 and Arg 37 of FGF1, respectively. These observations closely resemble those made in previous biochemical and structural studies^{8,9,12}.

In the linker between D2 and D3, the guanidinium moiety of invariant Arg 251 is surrounded by three hydrophobic FGF1 residues, Leu 89, Leu 133 and Pro 134, and is hydrogen bonded to the main chain of FGF1 His 93. These interactions immobilize the arginine side chain in the correct position to form a crucial hydrogen bond with the conserved Asn 95 of FGF1 (Fig. 4a). The importance of this interaction is highlighted by mutagenesis data that show a 400-fold reduction in receptor affinity when the equivalent asparagine in FGF2 is replaced by alanine¹⁸.

In domain D3, the conserved Arg 255 forms an ion pair with the invariant Glu 87 of FGF1 (Fig. 4a). Involvement of Glu 87 in a charge–charge interaction has been demonstrated by mutagenesis experiments that show a 10-fold reduction in receptor-binding affinity when glutamate is replaced by glutamine in FGF2 (ref. 19). Glu 87 is favourably positioned for interaction with Arg 255 by a hydrogen bond with neighbouring Tyr 97. Invariant Ile 257 of D3 packs hydrophobically against Leu 89 and His 93 and the main-chain atoms linking Glu 90 and Glu 91 of FGF1 and His 254 of the receptor (Fig. 4a). The only spliceform-specific FGF1–D3 interaction in the ternary complex is a hydrophobic contact between Val 51 of FGF1 and Ile 350 and Phe 352 of the receptor. The presence of a single contact with the spliceform-specific region of FGFR explains the lack of specificity of FGF1 towards different receptor isoforms.

Comparison of FGF–FGFR crystal structures with and without

heparin, obtained under similar crystallization conditions, shows that protein–protein interactions involved in crystal packing are partly conserved. The 3₁ screw axis in our crystals brings two D2 domains from different complexes together, forming a cleft between them in a fashion reminiscent of the canyon-forming interaction observed in crystals of FGF–FGFR complexes without heparin^{8,9}. This cleft was proposed to be the heparin-binding site in the FGF–FGFR–heparin ternary complex^{8,9}. In our structure a disaccharide of the heparin occupies the entry to the cleft, leaving it otherwise empty. Furthermore, analysis of crystal packing in FGF–FGFR complexes without heparin shows that the canyon-forming interaction between FGFR ectodomains is not observed when crystallization is achieved in a low salt buffer (compare PDB entry 1CVS with entries 1EVT and 1EV2). The crystallization process, and not heparin, is therefore likely to be responsible for the association of two FGFR molecules in a dimer with a canyon-like cleft.

Relative to its position in FGF–FGFR complexes without heparin^{8,9}, receptor domain D3 is swivelled around the linker region by 174.5° in A and by 163.3° in B (Fig. 4c). In the crystals neighbouring heteropentamers related by the 6₂ screw axis are linked through face-to-face packing of two D3 domains, involving a cluster of conserved hydrophobic residues, Ile 291, Val 311, Leu 343, Ile 350 and Phe 352 on β -strands G, F, C, C' (Fig. 5). It is possible that such an interaction may be involved in higher order FGFR oligomerization and the clustering observed in the focal adhesion complex²⁰.

The different receptor conformations observed in FGF–FGFR complexes with and without heparin suggest a mechanism to regulate receptor function. FGF and FGFR may initially associate in a binary complex with the receptor ectodomain in the conformation observed previously^{8,9}. Heparin binding would cause the D3 domain to rotate into the position observed in our structure through conformational changes in the linker, possibly involving Pro 253, which is in *trans* conformation in FGF–FGFR complexes without heparin^{8,9}, but adopts a *cis* conformation in the ternary complex (Fig. 4b). Indirect evidence in support of such a mechanism comes from the observation that the rare Ser252Phe FGFR2 mutation found in Apert syndrome is responsible for a severe phenotype similar to that of recurrent Ser252Trp, whereas Ser252Leu causes a normal phenotype²¹. Aromatic amino acids preceding a proline induce a high fraction of *cis* isomer in test peptides²². The severity of the Apert phenotype might thus be determined by the propensity of the Ser-252 mutation to stabilize the *cis* isomeric form of Pro 253.

We propose that our structure represents the active dimeric state of FGFR when bound to FGF and heparin. The role of heparin in receptor dimerization appears to be critical, as little protein–protein interface is present between the two halves of the heteropentamer. The absence of significant contacts between the two halves of the heteropentamer would facilitate heterodimerization of different ligand and receptor types. The asymmetric binding of heparin observed in the crystal is consistent with a stepwise assembly of the FGF signalling complex. The structure also suggests mechanisms for receptor activation, based on a heparin-induced conformational change in the receptor, and for higher order receptor oligomerization. The universality of the architecture of the FGF–FGFR–heparin signalling complex that emerges from this study will now have to be confirmed by structural determination of ternary complexes involving different members of the FGF family of ligands and receptors. □

Methods

Preparation of recombinant protein

We subcloned full-length human FGF1 complementary DNA into expression vector pET14a (Novagen), overexpressed the protein in a soluble form in *Escherichia coli* BL21(DE3) strain and purified it to homogeneity over a heparin Sepharose affinity column (Pharmacia). We subcloned human FGFR2 cDNA (splice variant IIIc) comprising

the extracellular immunoglobulin-like domains D2 and D3 (residues 148–366) into expression vector pET3a (Novagen), overexpressed it in *E. coli* BL21(DE3) strain as inclusion bodies, and refolded and purified it to homogeneity by a combination of standard chromatography techniques.

Preparation of heparin decasaccharide

Monodisperse heparin decasaccharide was prepared from a sample of heparin remaining from the 2nd International Standard. This material is highly homogeneous, containing more than 90% of the predominant repeating unit of heparin, the disaccharide α -1-*l*-IdoA(2OSO₃⁻)-(1→4)- α -D-GlcNSO₃⁻(6OSO₃⁻)-(1-. The parent heparin was partially degraded by brief incubation with heparin lyase 1 as described²³. The resulting oligosaccharides were separated by size-exclusion chromatography on a Biogel P10 column (1.6 × 100 cm) (BioRad) using 2% ammonium bicarbonate as eluent at 18 ml h⁻¹. Fractions (6 ml) were monitored by absorbance at 235 nm and pooled appropriately. The size of each oligosaccharide was confirmed by analytical size-exclusion chromatography.

Preparation of ternary complex and crystallization

The ternary complex of FGF1, FGFR2 and heparin was reconstituted by mixing the three components in 2:2:1 stoichiometric ratios and isolated by size-exclusion chromatography over a Superdex 200 HR 10/30 column (Pharmacia) as a single peak of *M*_r 83.6 kDa. Crystals were grown at 18° by the hanging drop method, mixing a 0.1 mM solution of ternary complex in 150 mM NaCl, 10 mM HEPES pH 7.2, 25 mM MgCl₂ with equal volumes of well solution containing 1.0 M Li₂SO₄, 0.1 M Tris-HCl pH 8.5, 10 mM NiSO₄. The crystals belong to space group *P*6₂ with unit-cell dimensions *a* = *b* = 195.90 Å, *c* = 68.86 Å, and contain one 2:2:1 complex per asymmetric unit with 72% solvent content. Crystals grown in the absence of NiSO₄ are isomorphous with the ones produced under the original conditions, but were too small for high-resolution X-ray analysis.

Phasing and refinement

The structure was determined by the multiple anomalous dispersion (MAD) method using selenomethionyl FGFR2 protein. MAD data at three different wavelengths near the Se K edge (Table 1) were collected at beamline 19-ID of the Structural Biology Center at the Advanced Photon Source, Chicago, US. The images were integrated and the intensities merged with HKL2000 (ref. 24). The positions of the eight selenium atoms in the asymmetric unit were determined with SHELX-97 (ref. 25). Phases were calculated in SHARP²⁶ and improved by SOLOMON²⁷. The resulting electron-density map at 3.5 Å resolution clearly showed the location of all components of the ternary complex. A homology-based model for FGFR2 domain D2 and a crystallographic FGF1 model (PDB entry 2AFG) were initially positioned in the experimental map. After a few cycles of phase combination and extension, a heparin decasaccharide²⁸ and a homology-based model for FGFR2 domain D3 were added. The structure was refined against native data measured at beamline 5.2 R of Elettra, Trieste, Italy, to 2.8 Å resolution. Refinement of the crystallographic model was carried out in CNS²⁹, alternated with manual rebuilding in O³⁰. Tight non-crystallographic symmetry restraints were individually applied to FGF1 and the D2 and D3 receptor domains throughout the refinement.

NMR studies of free heparin in solution show that the two main conformations of the iduronate ring, ¹C₄ chair and ²S₀ skew boat, are in equilibrium²⁸, and crystallographic studies of FGF2–heparin complexes reveal that both forms are present in protein-bound heparin⁶. The pyranose rings of the iduronate moieties in the heparin were kept in the ²S₀ skew boat conformation until a late phase of the refinement, when inspection of the density map warranted a switch to the ¹C₄ chair conformation for IdoA-1. Our assignment of the iduronate ring conformations must be considered tentative owing to the limited resolution of our study. Heparin lyase I digestion leaves an unsaturated iduronic acid at the non-reducing end of the heparin oligosaccharide. This chemical modification was not introduced in our model of the heparin molecule.

The refined model comprises 5,001 protein atoms, 175 heparin atoms, 41 water molecules, 5 sulphate ions and 5 nickel ions. 1.1% of the protein residues are in the generously allowed region and none in the disallowed region of the Ramachandran plot. Residues 1–9 (1–8 in B) and 139–140 of FGF1 and residues 148, 294–308 (294–309 in B) and 361–366 of FGFR2 are not visible in the electron-density map and have not been included in the final model. The quality of the electron-density map for residues 330–338 and 356–360 of FGFR2 is poor, indicating that they are partially disordered in the crystal. Residues for which no side-chain density was present were modelled as alanine during refinement.

Surface area accessibility calculations were carried out as implemented in CNS²⁹. Molecular superpositions and r.m.s.d. calculations were performed with LSQMAN. Figures were prepared with Molscript, Raster3D and GRASP.

Received 10 April; accepted 15 September 2000.

- Galzies, Z., Kinsella, A. R. & Smith, J. A. Fibroblast growth factors and their receptors. *Biochem. Cell Biol.* **75**, 669–685 (1997).
- Johnson, D. E. & Williams, L. T. Structural and functional diversity in the FGF receptor multigene family. *Adv. Cancer Res.* **60**, 1–41 (1993).
- Rapraeger, A. C., Kruka, A. & Olwin, B. B. Requirement of heparan sulfate for bFGF-mediated fibroblast growth and myoblast differentiation. *Science* **252**, 1705–1708 (1991).

- Spivak-Kroizman, T. *et al.* Heparin-induced oligomerization of FGF molecules is responsible for FGF receptor dimerization, activation and cell proliferation. *Cell* **79**, 1015–1024 (1994).
- Lin, X., Buff, E. M., Perrimon, N. & Michelson, A. M. Heparan sulfate proteoglycans are essential for FGF receptor signaling during *Drosophila* embryonic development. *Development* **126**, 3715–3723 (1999).
- Faham, S., Hileman, R. E., Fromm, J. R., Linhardt, R. J. & Rees, D. C. Heparin structure and interactions with basic fibroblast growth factor. *Science* **271**, 1116–1120 (1996).
- DiGabriele, A. *et al.* Structure of a heparin-linked biologically active dimer of fibroblast growth factor. *Nature* **393**, 812–817 (1998).
- Plotnikov, A. N., Schlessinger, J., Hubbard, S. R. & Mohammadi, M. Structural basis for FGF receptor dimerization and activation. *Cell* **98**, 641–650 (1999).
- Stauber, D., DiGabriele, A. & Hendrickson, W. Structural Interactions of fibroblast growth factor receptor with its ligands. *Proc. Natl Acad. Sci. USA* **97**, 49–54 (2000).
- Zhu, X. *et al.* Three-dimensional structure of acidic and basic fibroblast growth factor. *Science* **251**, 90–93 (1991).
- Thompson, L. D., Pantoliano, M. W. & Springer, B. A. Energetic characterization of the basic fibroblast growth factor-heparin interaction: identification of the heparin binding domain. *Biochemistry* **33**, 3831–3840 (1994).
- Springer, B. A. *et al.* Identification and concerted function of two receptor binding surfaces on basic fibroblast growth factor required for mitogenesis. *J. Biol. Chem.* **269**, 26879–26884 (1994).
- Kan, M. *et al.* An essential heparin-binding domain in the fibroblast growth factor receptor kinase. *Science* **259**, 1918–1921 (1993).
- Guimond, S., Maccarana, M., Olwin, B. B., Lindahl, U. & Rapraeger, A. C. Activating and inhibitory heparin sequences for FGF-2 (basic FGF). Distinct requirements for FGF-1, FGF-2, and FGF-4. *J. Biol. Chem.* **268**, 23906–23914 (1993).
- Ornitz, D. M. *et al.* Heparin is required for cell-free binding of basic fibroblast growth factor to a soluble receptor and for mitogenesis in whole cells. *Mol. Cell Biol.* **12**, 240–247 (1992).
- Sudhalter, J., Folkman, J., Svahn, C. M., Bergendal, K. & D'Amore, P. A. Importance of size, sulfation, and anticoagulant activity in the potentiation of acidic fibroblast growth factor by heparin. *J. Biol. Chem.* **264**, 6892–6897 (1989).
- Wang, F., Kan, M., Xu, J., Yan, G. & McKeenan, W. L. Ligand-specific structural domains in the fibroblast growth factor receptor. *J. Biol. Chem.* **270**, 10222–10230 (1995).
- Zhu, H. *et al.* Analysis of high-affinity binding determinants in the receptor binding epitope of basic fibroblast growth factor. *Protein Eng.* **10**, 417–421 (1997).
- Zhu, H. *et al.* Glu-96 of basic fibroblast growth factor is essential for high affinity receptor binding. Identification by structure-based site-directed mutagenesis. *J. Biol. Chem.* **270**, 21869–21874 (1995).
- Plopper, G. E., McNamee, H. P., Dike, L. E., Bojanowski, K. & Ingber, D. E. Convergence of integrin and growth factor receptor signaling pathways within the focal adhesion complex. *Mol. Biol. Cell* **6**, 1349–1365 (1995).
- Oldridge, M. *et al.* Genotype-phenotype correlation for nucleotide substitutions in the IgII–IgIII linker of FGFR2. *Hum. Mol. Genet.* **6**, 137–143 (1997).
- Reimer, U. *et al.* Side-chain effects on peptidyl-prolyl cis/trans isomerisation. *J. Mol. Biol.* **279**, 449–460 (1998).
- Rice, K. G., Kim, Y. S., Grant, A. C., Merchant, Z. M. & Linhardt, R. J. High-performance liquid chromatographic separation of heparin-derived oligosaccharides. *Anal. Biochem.* **150**, 325–331 (1985).
- Otwonowski, Z. & Minor, W. Processing of X-ray diffraction data collected in oscillation mode. *Methods Enzymol.* **276**, 307–326 (1997).
- Sheldrick, G. M. & Schneider, T. R. SHELXL: high resolution refinement. *Methods Enzymol.* **277**, 319–343 (1997).
- La Fortelle, E. d. & Bricogne, G. Maximum-likelihood heavy-atom parameter refinement in the MIR and MAD methods. *Methods Enzymol.* **276**, 472–494 (1997).
- Abrahams, J. P. & Leslie, A. G. W. Methods used in the structure determination of bovine mitochondrial F1 ATPase. *Acta Crystallogr. D* **52**, 30–42 (1996).
- Mulloy, B., Forster, M. J., Jones, C. & Davies, D. B. N.m.r. and molecular-modelling studies of the solution conformation of heparin. *Biochem. J.* **293**, 849–858 (1993).
- Brunger, A. T. *et al.* Crystallography & NMR system: A new software suite for macromolecular structure determination. *Acta Crystallogr. D* **54**, 905–921 (1998).
- Jones, T. A., Zou, J. Y., Cowan, S. W. & Kjeldgaard, M. Improved methods for binding protein models in electron-density maps and the location of errors in these models. *Acta Crystallogr. A* **47**, 110–119 (1991).

Acknowledgements

We would like to thank P. Gadhavi for discussions and early work on FGFR overexpression; D. Chirgadze, E. Parisini and J. Patel for help with X-ray data collection; R. Sanishvili for user support at the SBC beamline; M. Vinkovic for help with the use of SHELX; M. Hyvonen for advice on protein refolding and help with the figures; and M. Symmons for advice on production of selenomethionyl protein. We are grateful to S. Malcolm for insightful comments on the phenotype of FGFR mutations in Apert syndrome and for the FGFR2 cDNA, and to D. Fernig for the FGF1 cDNA. Heparin lyase I was a gift of K. Johansen, Leo Pharmaceuticals, Denmark. This research was supported by grants from the MRC and the Wellcome Trust. Use of the Argonne National Laboratory Structural Biology Center beamlines at the Advanced Photon Source was supported by the US Department of Energy, Basic Energy Sciences, Office of Science.

Correspondence and requests for materials should be addressed to L.P. (e-mail: luca@cryst.bioc.cam.ac.uk) or T.L.B. (e-mail: tom@cryst.bioc.cam.ac.uk). Coordinates have been deposited in the Protein Data Bank with accession number 1e0o.